Turkish Computational and Theoretical Chemistry

Turkish Comp Theo Chem (TC&TC)

Volume(Issue): 8(3) – Year: 2024 – Pages: 54-65

e-ISSN: 2602-3237

https://doi.org/10.33435/tcandtc.1334817

Received: 31.07.2023 ***Accepted:*** 09.12.2023 *Research Article*

Investigating the corrosion inhibition of copper using DFT theoretical study with three organic molecules

Boulanouar MESSAOUDI[a,b,1], Yazid DATOUSAID[a,c], Hadjer MISSOUM[c], Abbes BENCHADLI[b], Ismail Bilal CHATI[b], Tarik ATTAR[a,b]

[a] Ecole Supérieure en Sciences Appliquées de Tlemcen, ESSA-Tlemcen, BP 165 RP Bel Horizon, Tlemcen 13000, Algeria
[b]Laboratory of ToxicoMed, University of Abou Bekr Belkaïd, B.P.119, Tlemcen, 13000, Algeria
[c]Laboratory of Catalysis and Synthesis in Organic Chemistry, University of Tlemcen, Algeria

Abstract: A theoretical study of the inhibition efficiency of three 2,3,4-trisubstitutedthiophenes has been thoroughly probed using density functional theory B3LYP/6-31G(d) level. The calculated global quantities such as electrophilicity and nucleophilicity show that the three organic inhibitors are nucleophiles. The obtained values of charge transfer and energy of back-donation show that the 2-amino-4-(4-bromophenyl)thiophene-3-carbonitrile is the best inhibitor. Parr function indices have been calculated to determine the most preferred sites for the nucleophilic attacks towards the electrophilic transition metal surface of copper. The electrostatic surface potential has been mapped in order to explore the major regions of the molecules responsible of the inhibition. It is found that the zone surrounding the nitrogen atom and the π-aromatic system of benzene are the one forming the protection layer. The theoretical results are in good commitment with the experimental results.

Keywords: Corrosion, inhibition efficiency, B3LYP, Parr functions, ESP.

1. Introduction

Corrosion is a phenomenon that occurs when metals get in touch with an aggressive environment; resulting several consequences particularly in industry: renewal of corroded materials, loss of production, environmental pollution and serious accidents causing sometimes severe economic damages [1]. Most industrial equipment's can suffer from corrosion and must be designed with anti-corrosion treatments and matters.

To control and combat this undesirable phenomenon, various effective and preventive strategies have been developed: material selection, cathodic protection, coatings and the use of organic inhibitors [2]. The latest strategy appears to be the most practical and mildest.

In general, these inhibitors have shown good inhibition performance for many metals. In recent years rapid progress has been made in the synthesis of a variety of compounds such as quinols, quinoxalines, pyridiniums, triazoles and imidazolines [3]. Those molecules adsorb to the metal surface, by physical or chemical interactions blocking then one or more of the undesirable reactions occurring at the solution/metal interface and thus protecting the metal from dissolution [4]. This adsorption is carried out via heteroatoms such as nitrogen, oxygen, phosphorus and sulfur, triple bonds or even aromatic rings [5]. The Inhibition efficiency follows the sequence O < N < S < P as it has been cited in literature [6].

Among the heterocyclic molecules which are widely studied in corrosion protection are the derivatives of thiophene. These molecules offer a particular affinity for inhibiting metal corrosion in acid solutions [7]. As suggested by Bockris and Swinkels [8], this inhibition is caused by the great affinity of sulfur atom to the metal and it is easily

[1] Corresponding Authors

e-mail: messaoudiboulanouar@gmail.com

adsorbed on the metal surface by removing the water molecules readily existing on that surface.

Thiophenes and related compounds containing functional electronegative groups such as nitrile group and π-electrons in triple or conjugated double bonds are usually good inhibitors [9]. For example, a new benzothiophene-3-carbonitrile derivative has been reported as an effective copper corrosion inhibitor in hydrochloric acid. The structure of this inhibitor holds another additional nitrile group [10]. On the other hand, in recent years, theoretical chemistry and molecular simulation studies have been used to put in evidence a better understanding of some of the unknown properties of inhibitors interacting with metal surfaces. Calculations based on density functional theory have proved that they are very powerful tool for studying the electronic and structural properties of inhibitors [11-12].

The geometry of the inhibitor molecule in its fundamental state and the nature of their molecular orbitals (HOMO; highest occupied molecular orbital and LUMO; lowest unoccupied molecular orbital) are directly involved in the inhibiting properties of these molecules.

Several articles have appeared in the literature using DFT as a theoretical tool in correlating inhibition efficacy and electronic properties/molecular structures of organic compounds used as corrosion inhibitors. For instance, Benali et al. [13] investigated the carbon steel corrosion inhibition of 2-mercapto-1-methylimidazole (MMI) molecule in 1 M $HClO_4$ using DFT theoretical methods. Knowing that there are two forms thiol and thione for the (MMI), the HOMO and LUMO energies, energy gap, and dipole moment were calculated for both forms. The thione form was found to have the highest E_{HOMO} and dipole moment, and the lowest E_{LUMO} and energy gap values. In addition, Sahin et al. [14] conducted a study on the dependence of the inhibition efficiencies of three heterocyclic compounds namely: 3-amino-1,2,4-triazole (3-ATA), 4-hydroxy-2H-1-benzopyran-2-one (4-HQ), and 4-hydroxy-3-(1H-1,2,4-triazol-3-ylazo)-2H-1-benzopyran-2-one (3-ATA-Q) using B3LYP/6-31G(d) method. According to their theoretical data, a good agreement was found between experimental and theoretical data on the basis of several calculated parameters such as; HOMO and LUMO energies, energy gap, net atomic power, charges, dipole moments, and interaction energies.

The aim of this study is to investigate theoretically the inhibition efficacy of three organic heterocyclic molecules (Figure 1) on copper using DFT method and various theoretical approaches such as global and local indices, charge transfer, energy of back-donation.

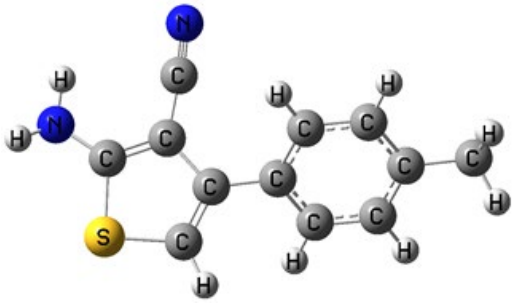

2-amino-4-*p*-tolylthiophene-3-carbonitrile

(**ATTC**)

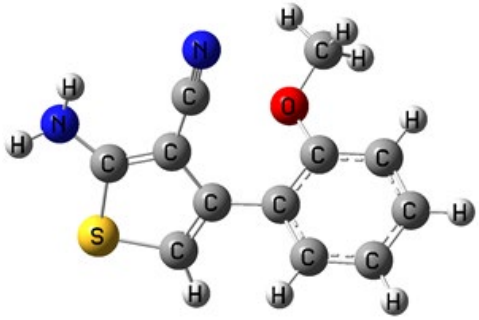

2-amino-4-(2-methoxyphenyl)thiophene-3-carbonitrile

(**AMTC**)

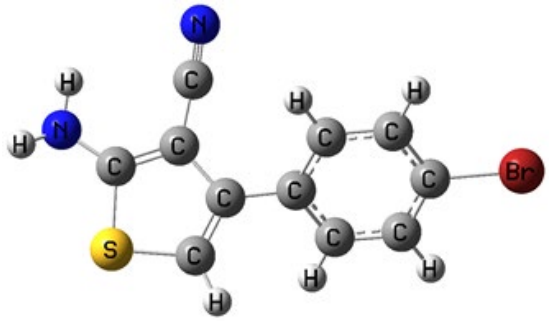

2-amino-4-(4-bromophenyl)thiophene-3-carbonitrile (**ABTC**)

Figure 1. Chemical structures of the studied inhibitors ATTC, AMTC, and ABTC.

2. Computational Method

The theoretical calculations have been performed using Gaussian 09 suite of program [15]. All the structures have been optimized and localized at B3LYP DFT method in conjunction with the basis set 6-31G(d) [16-20]. Each optimization has been followed by frequency calculation to check that each structure corresponds to a real minimum.

Within the standpoint of frontier molecular orbital theory, the ionization potential IP and electron affinity EA related to the highest occupied (HOMO) and lowest unoccupied molecular orbitals (LUMO) can be defined by the following equations [21]:

$$EA \approx -0.65E_{LUMO} - 0.38 \quad (1)$$

$$IP \approx -0.78E_{HOMO} + 3.17 \quad (2)$$

Hence, χ and η can be written as [22]:

$$\chi = -\frac{1}{2}(E_{LUMO} + E_{HOMO}) \quad (3)$$

$$\eta = \frac{1}{2}(E_{LUMO} - E_{HOMO}) \quad (4)$$

The electrophilic power of a given system is characterized by the electrophilicity index ω [23]:

$$\omega = \frac{\mu}{2\eta} \quad (5)$$

The nucleophilicity is defined by Domingo's group by the expression [24]:

$$N = E_{HOMO(Nu)} - E_{HOMO(TCE)} \quad (6)$$

where $E_{HOMO(TCE)}$ is the highest occupied molecular orbital energy of tetracyanoethylene (TCE) taken as reference since it presents the lowest HOMO energy.

In order to calculate Parr indices [25-30], the Mulliken atomic spin densities (ASD) were calculated and the following expressions were used [31]:

$$P_k^- = \rho_s^{rc}(k) \quad \text{for electrophilic attack} \quad (7)$$

$$P_k^+ = \rho_s^{ra}(k) \quad \text{for nucleophilic attack} \quad (8)$$

where $\rho_s^{rc}(k)$ is the cation atomic spin density, and $\rho_s^{ra}(k)$ is the anion atomic spin density.

Using P_k^+ and P_k^-, it is possible to define the local electrophilicity N_k and the local nucleophilicity N_k indices as follow:

$$\omega_k = \omega P_k^+ \quad (9)$$

$$N_k = N P_k^- \quad (10)$$

The number of transferred electrons (ΔN) was calculated as [32, 33]:

$$\Delta N = \frac{(\chi_{Cu} - \chi_{Inh})}{2(\eta_{Cu} + \eta_{Inh})} \quad (11)$$

where χ_{Cu} and χ_{Inh} are the absolute electronegativities, η_{Cu} and ηInh are the absolute hardness of copper and the inhibitor, respectively.

The theoretical value (χ_{Cu}=4.48 eV.mol^{-1}and η = 0 eV.mol^{-1}) for copper were obtained from the literature [34].

The interaction between the molecule acting as an inhibitor and the surface of a metal produces a charge transfer in the way of donation and back donation of charges. The back donation was calculated on the basis of the following expression [35-38]:

$$\Delta E_{back-donation} = -\frac{\eta}{4} \quad (12)$$

The charges transferred to the molecule, are energetically favored when $\eta > 0$ and $\Delta E_{back\text{-}donation} < 0$.

3. Results and discussion

In this investigation, we have opted for weight loss methods to capture a more accurate portrayal of uniform corrosion, mirroring real-world conditions with greater fidelity than electrochemical methods. Our approach aligned with the methodology outlined in Attar's prior work [39-40], conducting measurements in triplicate and calculating the mean weight loss value, which formed the basis of our analysis. To quantify the corrosion rate ('CR') and gauge the effectiveness of inhibitors, we employed the following equation [39]:

$$CR = \Delta w/(S \times t) \quad (13)$$

Where, the weight loss (Δw) is expressed in milligrams (mg), the sample area (S) is represented in square centimetres (cm^2), and the immersion time (t) is denoted in hours (h).

The corrosion inhibition efficiency (IE %) and surface coverage (θ) were derived from CR values using the equations [39]:

$$IE = 100 \times (CR - CR_{Inh})/CR \quad (14)$$

$$\theta = IE/100 \quad (15)$$

where CR represents the corrosion rate observed in the absence of the inhibitor, while CR_{inh} corresponds to the corrosion rate obtained in the presence of the inhibitor

Through experimental exploration, we established the optimal immersion time of 2 hours and a concentration of 10^{-3} g/L, as determined via gravimetric measurements conducted on copper in a 1M HNO_3 solution at the optimal temperature of 25°C. The inhibition efficiency values are reported in Table 1.

Table 1. Inhibition efficiency (IE) values of copper metal surface in 1 M HNO_3 at 10^{-3} mol/L concentration of the studied inhibitors (2 hours of immersion) at 298 K.

Inhibitors	IE %
2-amino-4-p-tolylthiophene-3-carbonitrile(ATTC)	83.11
2-amino-4-(2-methoxyphenyl)thiophene-3-carbonitrile (AMTC)	95.51
2-amino-4-(4-bromophenyl)thiophene-3-carbonitrile(ABTC)	96.54

Table 2. HOMO and LUMO energies, EA, IP, global reactivity indices μ, η, ω, N, gap, charge transfer, and the energy of back-donation for the three compounds at B3LYP/6-31G(d) level of theory.

	ATTC	AMTC	ABTC
E_{HOMO}(eV)	-5.68	-5.58	-5.88
E_{LUMO}(eV)	-0.79	-0.66	-1.10
EA (eV)	0.14	0.05	0.33
IP (eV)	7.60	7.53	7.76
ω (eV)	1.1	1.0	1.3
N (eV)	3.7	3.8	3.5
Gap (eV)	4.89	4.92	4.79
ΔN	0.79	0.77	0.83
$\Delta E_{back\text{-}donation}$(eV)	-1.22	-1.23	-1.20

ATTC

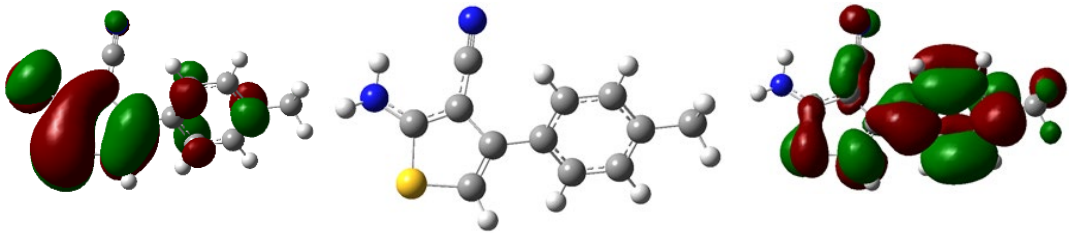

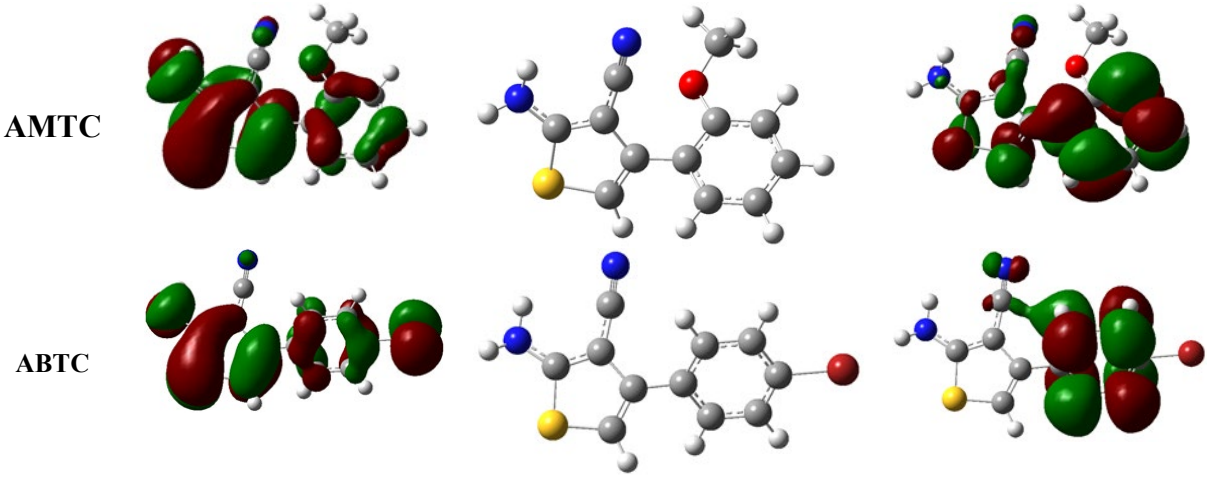

Figure 2. Frontier molecular orbitals HOMO/LUMO graphs for molecules ATTC, AMTC and ABTC.

As it can be seen in Table 1, the ABTC inhibitor shows excellent inhibition efficiency with respect to ATTC and AMTC compounds. The order of the experimental inhibition efficacy can be done as: IE_{ABTC}> IE_{AMTC}> IE_{ATTC}. In the following subsection, several theoretical approaches will be deployed to investigate the experimental findings cited above.

3.1. Global reactivity index

The quantum chemical calculation of the highest occupied molecular orbital (HOMO) and lowest unoccupied molecular orbital (LUMO) energies as well as global quantities i.e. chemical potential μ, hardness η, electrophilicity ω, and nucleophilicity N are given in Table 2.

The nucleophilicity values vary from 3.5 for molecule ABTC to 3.8 for AMTC. These values are about three times greater than electrophilicity ones that are about 1 unit. Basically, this means that the inhibitor molecules are nucleophiles and then can exchange electrons with the copper transition metal ions (acceptors) as donors.

Corrosion inhibition efficiency has to do with the HOMO energy. The inhibition efficiency of inhibitors increases as the energy of HOMO increases as well.

The HOMO explains the capacity of a given molecule to donate electrons. The HOMO energy order goes as: E_{AMTC}>E_{ATTC}> E_{ABTC}. The three molecules have additional electrons; oxygen, nitrogen and benzene ring, and thus have the ability to give unshared pairs of electrons to the empty orbitals of copper atoms (d-orbitals).

It is worthy to note here that the energy gap value is little bit larger and is in the same order of magnitude, where ΔE_{AMTC}>ΔE_{ATTC}>ΔE_{ABTC}. In fact, the inhibition efficiency increases with the decrease in energy gap of the frontier molecular orbitals. Therefore, it can be said that the inhibitor ABTC having the lowest gap presents the highest inhibition efficiency. This is quite obvious since this compound has a bromine halogen atom in addition to nitrogen atoms. This is in good agreement with the experimental study since the copper metal surface is electrophile and then its adhesion to the inhibitor will produce a protection layer against the acidic media.

The HOMO and LUMO density distribution of the three molecules are shown in Figure2.

It is clear that the HOMO is located mainly on the region surrounding sulfur atom, while the LUMO is located on the benzene part of the molecules and this for all the inhibitors.

This leads to say that the region surrounding the sulfur atom will be the one responsible of reaction with the copper surface.

The charge transfer ΔN is of the order of 1unit for the three inhibitors. This fraction of electrons transferred is lower than 3.6, so the three inhibitors can be considered as strong electron donors. The order of charge transfer is: ΔN_{ABTC}>ΔN_{ATTC}>ΔN_{AMTC}. The inhibitor ABTC has the highest ΔN and is considered to have the highest inhibition efficiency. Hence, increasing electron-donating capacity at the metal surface means an increasing in the inhibition efficiency.

In addition, the back-donation energy calculated value is negative which means that the charge

transfer to the entitled inhibitors under study is energetically favored. This energy decreases in the following order: $\Delta N_{ABTC}>\Delta N_{ATTC}>\Delta N_{AMTC}$. This indicates that the back-donation is much favored for inhibitor ABTC and is, by this, the best inhibitor.

3.2. Local reactivity index

On the other hand, calculation of Parr function indices is very interesting and important in terms of locating the most reactive sites i.e. nucleophilic and electrophilic sites of a given molecule. The sites of the molecules with higher values of P_k^+ are electron poor sites and tend to be attacked by electron abundant atoms of another molecule. On the contrary, the positions of the molecules which have higher values of P_k^- are nucleophilic sites and can interact with electron poor positions of another molecule. Thus, it can be possible the determination atoms responsible and even the area of the reaction and in our case the ones that form the protection layer with copper metal.

The calculated Parr functions for the studied inhibitors are displayed in following Tables 3-5.

Table 3. Parr functions $\mathbf{P_k^+}$, $\mathbf{P_k^-}$, local electrophilicity $\boldsymbol{\omega_k^+}$ and local nucleophilicity $\mathbf{N_k}$ of inhibitor ATTC using Mulliken ASD at B3LYP/6-31G(d).

Atom k	P_k^+	P_k^-	ω_k^+	N_k
C1	0.07103	0.03322	0.07614	0.12251
C2	0.11064	0.10648	0.11861	0.39264
C3	0.04307	0.02745	0.04617	0.10121
C4	-0.01035	-0.00391	-0.01109	-0.01440
C5	0.17826	0.13952	0.19110	0.51446
C6	-0.03476	-0.00706	-0.03727	-0.02603
C11	-0.05769	0.03478	-0.06184	0.12823
C12	0.24308	0.09709	0.26059	0.35800
C13	-0.01635	-0.00614	-0.01753	-0.02264
N17	0.02167	0.16643	0.02323	0.61371
C20	0.01745	-0.01689	0.01871	-0.06230
N21	-0.00161	0.02990	-0.00172	0.11025
S22	0.09371	0.01576	0.10047	0.05811
C23	0.00415	-0.01530	0.00445	-0.05640
C24	0.33127	0.41011	0.35514	1.51225

Table 4. Parr functions $\mathbf{P_k^+}$, $\mathbf{P_k^-}$, local electrophilicity $\boldsymbol{\omega_k^+}$ and local nucleophilicity $\mathbf{N_k}$ of inhibitor AMTC using Mulliken ASD at B3LYP/6-31G(d).

Atom k	P_k^+	P_k^-	ω_k^+	N_k
C1	0.02769	0.08503	0.02746	0.32172
C2	0.10994	0.11807	0.10903	0.44673
C3	0.09582	-0.05595	0.09503	-0.21169
C4	-0.04547	0.11320	-0.04510	0.42829
C5	0.20843	0.05046	0.20670	0.19091
C6	0.00313	-0.01081	0.00310	-0.04091
C10	-0.04243	0.05001	-0.04208	0.18920
C11	0.21878	0.08306	0.21697	0.31426
N12	0.00969	0.15554	0.00961	0.58848
C15	0.01563	-0.02508	0.01550	-0.09488
N16	-0.00081	0.04714	-0.00081	0.17835
S17	0.10692	0.00715	0.10604	0.02706
C18	0.00092	-0.02497	0.00091	-0.09446
C19	0.28048	0.33572	0.27816	1.27018
O22	0.00190	0.09394	0.00189	0.35543
C23	0.00097	-0.00573	0.00096	-0.02168

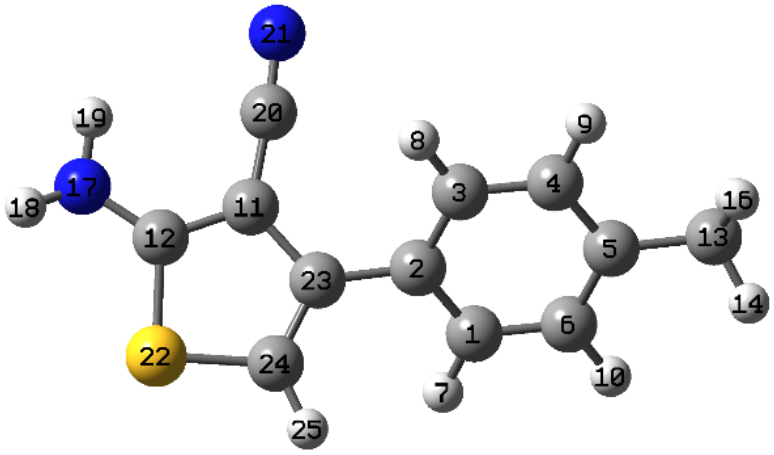

Figure 3. Atom numbering for inhibitor ATTC.

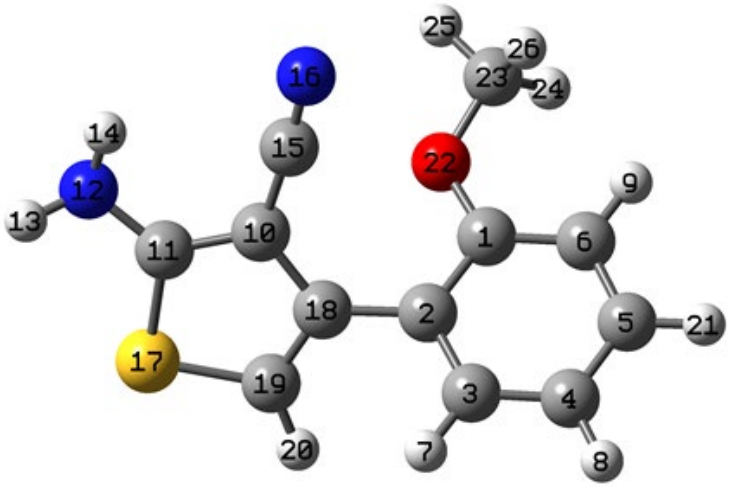

Figure 4. Atom numbering for inhibitor AMTC.

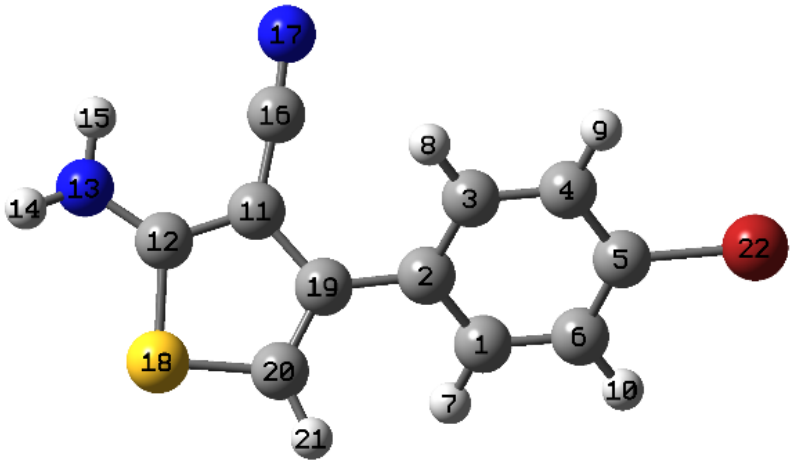

Figure 5. Atom numbering for inhibitor ABTC.

Table 5. Parr functions P_k^+, P_k^-, local electrophilicity ω_k^+ and local nucleophilicity N_k of inhibitor ABTC using Mulliken ASD at B3LYP/6-31G(d).

Atom k	P_k^+	P_k^-	ω_k^+	N_k
C1	0.07766	0.02294	0.09872	0.07997
C2	0.15053	0.09167	0.19137	0.31956
C3	0.05179	0.01822	0.06584	0.06350
C4	-0.00422	0.00318	-0.00536	0.01108

C5	0.21937	0.09892	0.27888	0.34485
C6	-0.02983	0.00026	-0.03792	0.00090
C11	-0.04640	0.04344	-0.05899	0.15143
C12	0.15514	0.09152	0.19723	0.31904
N13	0.01437	0.16860	0.01827	0.58777
C16	0.01133	-0.01904	0.01440	-0.06639
N17	-0.00884	0.03354	-0.01123	0.11694
S18	0.08446	0.01324	0.10737	0.04614
C19	0.01027	-0.01791	0.01306	-0.06242
C20	0.33352	0.39006	0.42399	1.35978
Br22	0.00283	0.09012	0.00360	0.31418

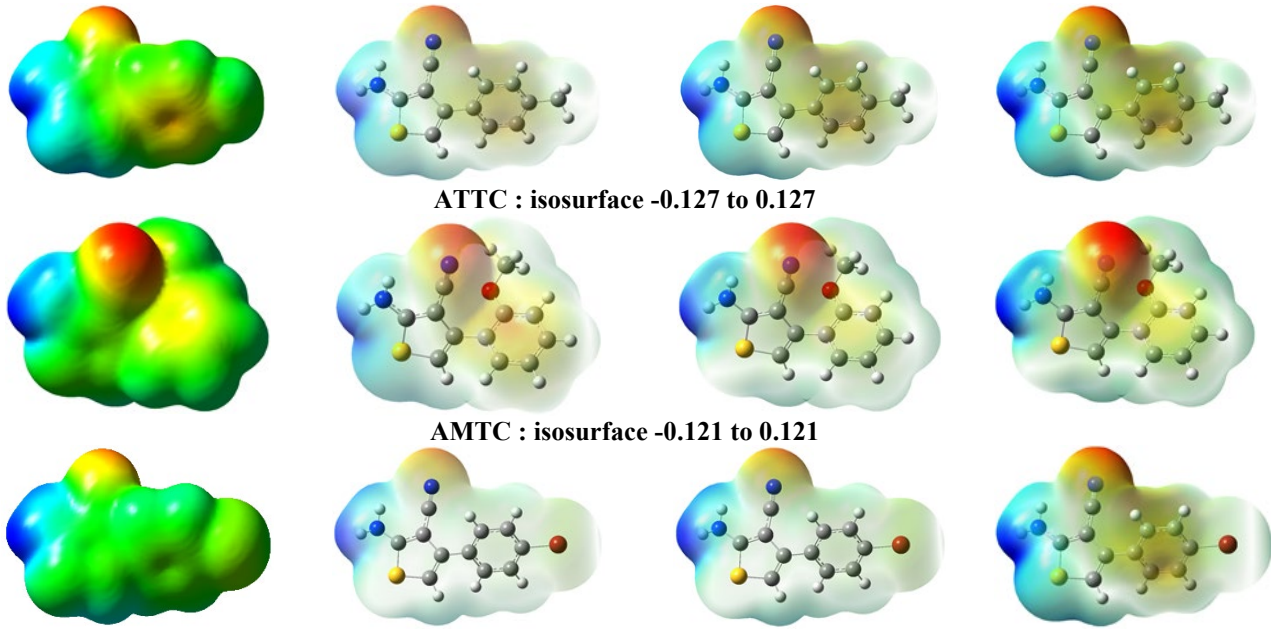

Figure 6. ESP map visualization for studied inhibitors ATTC, AMTC, and ABTC.

Table 6. Values of energy, enthalpy, Gibbs free energy, and entropy calculated in the gas phase at B3LYP/6-31G(d).

	ΔE (eV)	ΔH (eV)	ΔG (eV)	ΔS (cal.K^{-1}.mol^{-1})
ATTC	-26421,78	-26416,18	-26417,72	119.338
AMTC	-28468,16	-28462,40	-28463,97	121.133
ABTC	-95315,74	-95311,17	-95312,70	118.749

As it can be seen in Table 4, the values of Parr local reactivity indices show that the N12, and C19 sites are the most favored positions for the nucleophilic attack. Nevertheless, the carbon atoms C1, C2, and C4 are the most nucleophilic of the benzene cycle and ought to contribute in the adhesion on the copper surface.

From the results for the local reactivity descriptors N_k shown in Table 5, it can be concluded the N13, and C20 exhibit the highest values and thus will be preferred sites for a nucleophilic attack. However, the positions C2, C5 and Br22 of the conjugated system of benzene seem to have the most nucleophilic sites.

3.3. Electrostatic potential

Electrostatic potential (ESP) map for the studied structures is shown in Figure 6. The blue and red colored spheres correspond to ESP varying from minimum to maximum level [41-45].

The negative ESP regions are indicated in red, while the positive regions in blue. The potential

surface provides a useful visualization of the total charge distribution for a given molecule, subdivided to many colored regions coded in the order: red < orange < yellow < green < blue, indicating the most negative part (red) to the most positive one (blue) in order to identify different potentials.

As it is depicted in Figure 6, the most negative areas are mostly localized on the nitrogen atom belonging to –CN group and the very nearest surrounding area going down the benzene moiety. This effect corresponds to the abundant π-electron cloud and aggregation of electron density due to the nitrile triple bond. However, the most positive zones are observed at the nitrogen atom of–NH_2 group and its immediate neighboring region.

3.4. Thermodynamics calculations

The calculated values of different thermodynamics energy are listed in Table 6.

As it is listed in Table 6, Gibbs free energy calculation of the inhibitors show that the energy order is: $\Delta G_{ATTC}>\Delta G_{AMTC}>\Delta G_{ABTC}$, so that the order of reactivity can be done as: ATTC>AMTC>ABTC meaning that ATTC molecule is the least stable one and most reactive, whereas inhibitor ABTC is the most stable and then is the least reactive one.

3.5. The suggested inhibition mechanism

The adsorption mechanism of the organic molecules acting as corrosion inhibitors follows some steps. The studied inhibitors can adsorb on the metal surface through replacement of water molecules [46].

$$Inhibitor_{(soln)} + xH_2O_{(ads)} \rightarrow Inhibitor_{(ads)} + H_2O_{(soln)}$$

$$Cu \rightarrow Cu^{+2} + 2e^-$$

$$Cu^{+2} + Inhibitor_{(ads)} \rightarrow [Cu - Inhibitor]^{+2}{}_{(ads)}$$

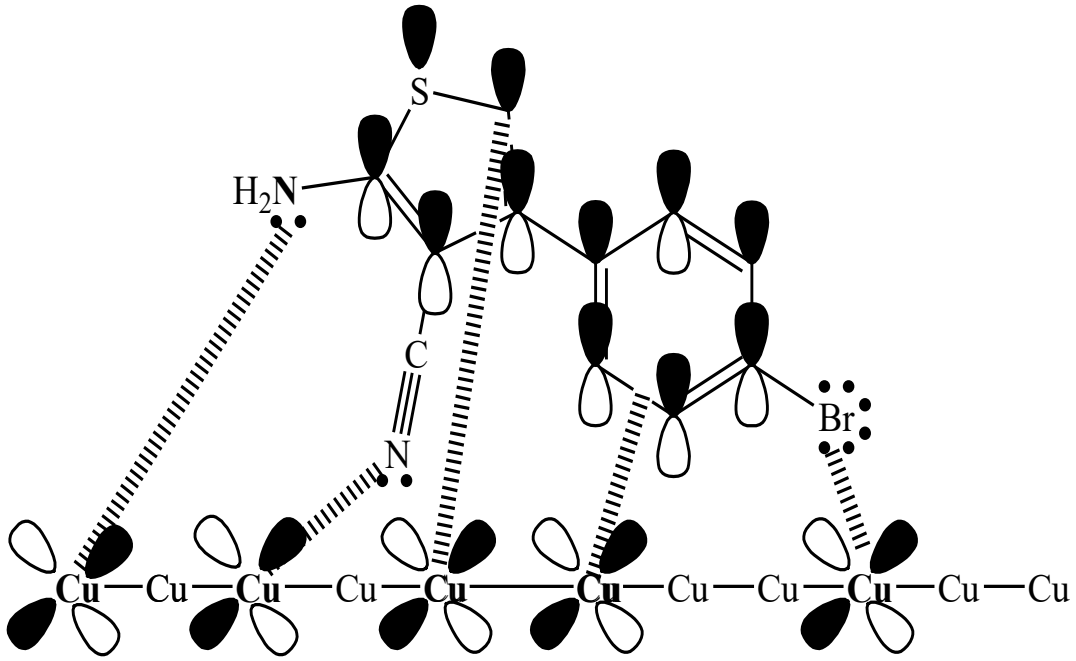

Figure 7. Schematic presentation of the suggested mechanism for the adsorption of the studied inhibitors on the copper surface.

Metal ions Cu^{+2} can coordinate with the inhibitor molecules to produce a copper-inhibitor complex that forms the protection layer of copper against the corrosion media (acid) [47]. The type of adsorption of the organic inhibitor on the metal surface is directly related to the type of interaction between the metal surface and inhibitor molecules. The studied molecules contain nitrogen atoms as donors of electrons and the benzene rings, which lead to form an efficient adsorption mechanism.

On the basis of the obtained results shown previously, the adsorption of the three studied inhibitors on copper metal surface can be schematized as:

4. Conclusions

In this study, a theoretical study at B3LYP/6-31G(d) has been done to explore the inhibition efficiency of some organic molecules on copper metal using different approaches. The obtained results show that the three studied molecules exhibit a nucleophilic character. Parr functions analysis show that the nitrogen, bromine and some carbon atoms especially the ones of the benzene aromatic cycle are the most reactive sites to attack the metal surface. ESP investigation reveals and demonstrates clearly the most nucleophilic region is located on nitrogen atom and the area surrounding the benzene ring to be the donor of electrons to the poor electrophilic transition metal surface of copper. Among the three studied organic compounds, the inhibitor 2-amino-4-(4-bromophenyl)thiophene-3-carbonitrile (ABTC) displayed the lowest energy gap, the highest charge transfer and back-donation energy indicating that it is a strong electron donor and has the best inhibition efficiency. The inhibitor ABTC presents effective anti-corrosion potential. The thermodynamics results show a good stability of the inhibitors studied. The results of quantum chemical calculations using B3LYP/6-31G(d) level of theory comply well with the available experimental data.

References

[1] A. H. Al-Moubaraki, I. B. Obot, Corrosion challenges in petroleum refinery operations: Sources, mechanisms, mitigation, and future outlook. Journal of Saudi Chemical Society 25 (2021) 101370.

[2] A. El-Meligi, Corrosion preventive strategies as a crucial need for decreasing environmental pollution and saving economics. Recent Patents on Corrosion Science 2 (2010) 22-33.

[3] A.Chaouiki, H. Lgaz, I. M. Chung, et al., Understanding corrosion inhibition of mild steel in acid medium by new benzonitriles: Insights from experimental and computational studies. Journal of Molecular Liquids 266 (2018) 603-616.

[4] M. V. Fiori-Bimbi, P. E. Alvarez, H. Vaca, et al., Corrosion inhibition of mild steel in HCl solution by pectin. Corrosion Science 92 (2015) 192-199.

[5] M. Bouklah, N. Benchat, B. Hammouti, et al., Thermodynamic characterisation of steel corrosion and inhibitor adsorption of pyridazine compounds in 0.5 M H_2SO_4. Materials Letters 60 (2006) 1901-1905.

[6] M. Bouklah, B. Hammouti, A. Aouniti, et al., Thiophene derivatives as effective inhibitors for the corrosion of steel in 0.5 M H_2SO_4. Progress in Organic Coatings 49 (2004) 225-228.

[7] L. Guo, Z. S. Safi, S. Kaya, et al., Anticorrosive effects of some thiophene derivatives against the corrosion of iron: A computational study. Frontiers in Chemistry 6 (2018) 155-160.

[8] J. M. Bockris, D. Swinkels, The relative electrocatalytic activity of noble metals in the oxidation of ethylene. Journal of The Electrochemical Society 111 (1964) 736.

[9] P. K. Yadav, O. Prakash, B. Ray, et al., Functionalized polythiophene for corrosion inhibition and photovoltaic application. Journal of Applied Polymer Science 138 (2021) 51306.

[10] A. Fouda, A. Attia, A. Negm, Some thiophene derivatives as corrosion inhibitors for carbon steel in hydrochloric acid. Journal of Metallurgy 2014 (2014) 1-15.

[11] D. K. Verma, Density functional theory (DFT) as a powerful tool for designing corrosion inhibitors in aqueous phase. Advanced Engineering Testing 87 (2018).

[12] T. Attar, F. Nouali, Z. Kibou, et al., Corrosion inhibition, adsorption and thermodynamic properties of 2-aminopyridine derivatives on the corrosion of carbon steel in sulfuric acid solution. Journal of Chemical Sciences 133 (2021) 109-118.

[13] O. Benali, I. Larabi, M. Traisnel, et al., Electrochemical, theoretical and XPS studies of 2-mercapto-1-methylimidazole adsorption on carbon steel in 1 M HClO4. Applied Surface Science 253 (2007) 6130-6139.

[14] M. Sahin, G. Gece, E. Karei, et al., Experimental and theoretical study of the effect of some heterocyclic compounds on the corrosion of low carbon steel in 3.5% NaCl medium. Journal of Applied Electrochemistry 38 (2008) 809-815.

[15] M. J. Frisch, G. W. Trucks, H. B. Schlegel, et al., Gaussian 09, Inc., Wallingford CT, (2009).

[16] R. G. Parr, W. Yang, Density-functional theory of atoms and molecules. Oxford Univ. Press, Oxford, (1989).

[17] J. A. Pople, P. M. W. Gill, B. G. Johnson, Kohn-Sham density-functional theory within a finite basis set. Chemical Physics Letter 199 (1992) 557-60.

[18] J. Tirado-Rives, W. L. Jorgensen, Performance of B3lyp density functional methods for a large set of organic molecules. Journal of Chemical Theory and Computation 2 (2008) 297-306.

[19] L. Lu, Can B3LYP be improved by optimization of the proportions of exchange and correlation functionals? International Journal of Quantum Chemistry 115 (2015) 471-476.

[20] F. Islam, M. R. Rahman, M. M. Matin, The effects of protecting and acyl groups on the conformation of benzyl α-L-rhamnopyranosides: An in silico study. Turkish Computational and Theoretical Chemistry 5 (2021) 39-50.

[21] N. V. Bondarev, K. P. Katin, V. B. Merinov, et al., Probing of Neural Networks as a Bridge from Ab Initio Relevant Characteristics to Differential Scanning Calorimetry Measurements of High-Energy Compounds. Physica Status Solidi (RRL)–Rapid Research Letters 16 (2022) 2100191.

[22] T. Attar, A. Benchadli, B. Messaoudi, et al., Experimental and theoretical studies of eosin Y dye as corrosion inhibitors for carbon steel in perchloric acid solution. Bulletin of Chemical Reaction Engineering & Catalysis 15 (2020) 454-464.

[23] P. K. Chattaraj, U. Sarkar, D. R. Roy, Electrophilicity index. Chemical Review 106 (2006) 2065-2091.

[24] L. R. Domingo, P. Pérez, The nucleophilicity N index in organic chemistry. Organic & Biomolecular Chemistry 9 (2011) 7168-7175.

[25] R.G. Parr, W. Yang, Density functional approach to the frontier-electron theory of chemical reactivity. Journal of American Chemical Society 106 (1984) 4049-4050.

[26] L. R. Domingo, P. Pérez, J. A. Sáez, Understanding the local reactivity in polar organic reactions through electrophilic and nucleophilic Parr functions. RSC advances 3 (2013) 1486-1494.

[27] S. Jorio, M. Salah, H. Abou El Makarim, et al., Reactivity indices related to DFT theory, the electron localization function (ELF) and non-covalent interactions (NCI) calculations in the formation of the non-halogenated pyruvic esters in solution. Mediterranean Journal of Chemistry 8 (2019) 476-485.

[28] M. Zoubir, A. Zeroual, M. El Idrissi, et al., Understanding the chemoselectivity and stereoselectivity in Michael addition reactions of β-hydroxyparthenolides and amines such as pyrrolidine, morpholine, piperidine and 1-methylpiperazine: a DFT study. Journal of Materials and Environmental Science 8 (2017) 990-996.

[29] M. S. M. Ahmed, A. E. Mekky, S. M. Sanad, Regioselective [3+2] cycloaddition synthesis and theoretical calculations of new chromene-pyrazole hybrids: A DFT-based Parr Function, Fukui Function, local reactivity indexes, and MEP analysis. Journal of Molecular Structure 1267 (2022) 133583.

[30] L. R. Domingo, M. Ríos-Gutiérrez, Application of reactivity indices in the study of polar Diels-Alder reactions. Conceptual density functional theory: Towards a new chemical reactivity theory 2 (2022) 481-502.

[31] P. Fuentealba, J. Melin, Atomic spin-density polarization index and atomic spin-density information entropy distance. International Journal of Quantum Chemistry 90 (2002) 334-341.

[32] I. Lukovits, E. Kalman, F. Zucchi, Corrosion inhibitors-correlation between electronic structure and efficiency. Corrosion 57 (2001) 3-8.

[33] L. Guo, S. Zhu, S. Zhang, et al., Theoretical studies of three triazole derivatives as corrosion inhibitors for mild steel in acidic medium. Corrosion Science 87 (2014) 366-375.

[34] A. Zarrouk, B. Hammouti, A. Dafali, et al., A theoretical study on the inhibition efficiencies of some quinoxalines as corrosion inhibitors of copper in nitric acid.

Journal of Saudi Chemical Society 18(2014) 450-455.

[35] H. Herrera-Hernández, M. Abreu-Quijano, M. Palomar-Pardavé, et al., Quantum chemical study of 2-mercaptoimidazole, 2-mercaptobenzimidazole, 2-mercapto-5-methylbenzimidazole and 2-mercapto-5-nitrobenzimidazole as corrosion inhibitors for steel. International Journal of Electrochemical Science 6 (2011) 3729-3742.

[36] S. Cao, D. Liu, H. Ding, et al., Task-specific ionic liquids as corrosion inhibitors on carbon steel in 0.5 M HCl solution: An experimental and theoretical study. Corrosion Science 153 (2019) 301-313.

[37] E. A. M. Gad, E. M. S. Azzam, S. A. Halim, Theoretical approach for the performance of 4-mercapto-1-alkylpyridin-1-ium bromide as corrosion inhibitors using DFT. Egyptian journal of petroleum 27 (2018) 695-699.

[38] H. Kumar, V. Yadav, A. Kumari, Adsorption, corrosion inhibition mechanism, and computational studies of Azadirachtaindica extract for protecting mild steel: Sustainable and green approach. Journal of Physics and Chemistry of Solids 165 (2022) 110690.

[39] T. Attar, A. Benchadli, B. Messaoudi, et al., Corrosion inhibition, adsorption and thermodynamic properties of poly (sodium 4-styrenesulfonate) on carbon steel in phosphoric acid medium. French-Ukrainian Journal of Chemistry 10 (2022) 70-83.

[40] T. Attar, A. Benchadli, B. Messaoudi, et al., Corrosion inhibition efficiency, experimental and quantum chemical studies of neutral red dye for carbon steel in perchloric acidic media. Chemistry & Chemical Technology 16 (2022) 440-447.

[41] M. Atilhan, T. Altamash, S. Aparicio, Quantum chemistry insight into the interactions between deep eutectic solvents and SO2. Molecules 24 (2019) 2963.

[42] F. Zhang, B. Liu, G. Liu, et al., Substructure-activity relationship studies on antibody recognition for phenylurea compounds using competitive immunoassay and computational chemistry. Scientific Reports 8 (2018) 3131.

[43] P. C. Rathi, R. F. Ludlow, M. L. Verdonk, Practical High-Quality Electrostatic Potential Surfaces for Drug Discovery Using a Graph-Convolutional Deep Neural Network. Journal of Medicinal Chemistry 63 (2020) 8778-8790.

[44] Y. M. Chai, H. B. Zhang, X. Y. Zhang, et al., X-ray structures, spectroscopic, antimicrobial activity, ESP/HSA and TD/DFT calculations of Bi (III) complex containing imidazole ring. Journal of Molecular Structure 1256 (2022) 132517.

[45] S. Boukhssas, Y. Aouine, H. Faraj, et al., Hirshfeld Surface Analysis and DFT calculations of 1-phenyl-N- (benzomethyl)-N-({1-[(2-benzo-4-methyl-4,5-dihydro-1,3-oxazol-4-yl)methyl]- 1H-1,2,3-triazol-4-yl}methyl)methanamine. Journal of Materials and Environmental Sciences 9 (2018) 2254-2262.

[46] A. Al-Amiery, T. A. Salman, K. F. Alazawi, et al., Quantum chemical elucidation on corrosion inhibition efficiency of Schiff base: DFT investigations supported by weight loss and SEM techniques. International Journal of Low-Carbon Technologies 15 (2020) 202-209.

[47] E. E. Oguzie, Y. Li, F. H. Wang, Corrosion inhibition and adsorption behavior of methionine on mild steel in sulfuric acid and synergistic effect of iodide ion. Journal of Colloid and Interface Science 310 (2007) 90-98.

SUPPLEMENTAL INFORMATION

Investigating the corrosion inhibition of copper using DFT theoretical study with three organic molecules

Boulanouar MESSAOUDI[a,b], Yazid DATOUSAID[a,c], Hadjer MISSOUM[c], Abbes BENCHADLI[b], Ismail Bilal CHATI[b], Tarik ATTAR[a,b]

[a] *Ecole Supérieure en Sciences Appliquées de Tlemcen, ESSA-Tlemcen, BP 165 RP Bel Horizon, Tlemcen 13000, Algeria*

[b]*Laboratory of ToxicoMed, University of Abou Bekr Belkaïd, B.P.119, Tlemcen, 13000, Algeria*

[c]*Laboratory of Catalysis and Synthesis in Organic Chemistry, University of Tlemcen, Algeria*

[*]Corresponding author: messaoudiboulanouar@gmail.com

Pages **Contents**

Optimized molecular structures of the three organic inhibitors at B3LYP/6-31G(d) level of theory.

ATTC molecule

```
0 1
 C                  1.68709100   -1.26733000   -0.57558800
 C                  0.86454400   -0.30763700    0.03717400
 C                  1.48222100    0.79836600    0.64293000
 C                  2.86867800    0.93213000    0.63496200
 C                  3.69081800   -0.02481800    0.02675200
 C                  3.07229000   -1.12903300   -0.57429900
 H                  1.23216700   -2.11858000   -1.07464800
 H                  0.88000700    1.55306100    1.13840400
 H                  3.31997800    1.79683200    1.11622700
 H                  3.68379100   -1.88707500   -1.05895800
 C                 -1.57900600    0.58106700   -0.07514200
 C                 -2.89288700    0.13597400   -0.01465200
 C                  5.19122600    0.14458600   -0.00819700
 H                  5.70418400   -0.82257900   -0.04143100
 H                  5.50662900    0.71047400   -0.89516000
 H                  5.55354700    0.69071400    0.86932200
 N                 -4.03358900    0.87908000   -0.20482500
 H                 -4.86740300    0.57642100    0.28159800
H                 -3.89434700    1.88334700   -0.17621000
 C                 -1.31534700    1.96123400   -0.27406600
 N                 -1.18940900    3.11120000   -0.42526100
 S                 -2.95881900   -1.59331100    0.20124000
 C                 -0.60269300   -0.48758300    0.05978000
 C                 -1.21222100   -1.69816200    0.22392900
 H                 -0.74476200   -2.65435700    0.41012000
```

AMTC molecule

```
0 1
 C                  1.82035300    0.32066100   -0.36119500
 C                  0.99551300   -0.74530700    0.06866500
 C                  1.60418900   -1.86498200    0.64806000
 C                  2.98737000   -1.94063400    0.81695300
 C                  3.78219500   -0.87316600    0.40728900
 C                  3.20569700    0.25579900   -0.17900700
 H                  0.96892500   -2.67559200    0.99388500
 H                  3.43313500   -2.81701600    1.27786200
 H                  3.83928700    1.07388600   -0.50153500
 C                 -1.33919200    0.38078700    0.34344400
 C                 -2.68445100    0.13168800    0.11981800
 N                 -3.74485600    0.97590900    0.36518900
 H                 -4.62162400    0.53933900    0.62075100
 H                 -3.51528800    1.76998500    0.95381300
 C                 -0.94070100    1.56883000    1.01022700
 N                 -0.70490700    2.55957100    1.57884300
 S                 -2.91778800   -1.41859900   -0.64696300
```

```
 C                 -0.47535400   -0.70148700   -0.09668100
 C                 -1.19474000   -1.72945400   -0.63100900
 H                 -0.81832200   -2.65153400   -1.05041100
H                  4.86007100   -0.90886300    0.54141100
 O                  1.18114700    1.35978700   -0.96670500
 C                  1.90790600    2.55265100   -1.22432400
 H                  2.69170400    2.39092900   -1.97590000
 H                  1.17825400    3.26568900   -1.61060000
 H                  2.35492100    2.95179300   -0.30588400
```

ABTC molecule

```
0 1
 C                  0.60421800   -1.31197600   -0.57842700
 C                 -0.20058000   -0.33517000    0.03224300
 C                  0.43162800    0.76801800    0.62918700
 C                  1.81972200    0.89102800    0.62287800
 C                  2.59045700   -0.09847700    0.01699800
 C                  1.99255100   -1.20349300   -0.58614100
 H                  0.13567400   -2.15635800   -1.07548800
 H                 -0.15857600    1.53728100    1.11569600
 H                  2.29664600    1.74641100    1.08843300
 H                  2.60255900   -1.96117100   -1.06591000
 C                 -2.63031900    0.58999200   -0.07589100
 C                 -3.95030400    0.16267400   -0.01161500
 N                 -5.07966200    0.92065400   -0.19786700
 H                 -5.92293400    0.62380700    0.27520300
 H                 -4.93143500    1.92350300   -0.17111200
 C                 -2.34559300    1.96556400   -0.27596900
 N                 -2.19634900    3.11282000   -0.42611600
 S                 -4.03920500   -1.56561600    0.20735100
 C                 -1.67026600   -0.49288100    0.05671300
 C                 -2.29527600   -1.69529600    0.22339900
H                 -1.84096200   -2.65779600    0.40997200
Br                 4.49431300    0.06628500    0.00437800
```